energies

MDPI

Article

Digital Twin Development of a Dynamic Hardware Emulator

Sandro Kellermüller *, Artjoms Obushevs *, Miguel Ramirez Gonzalez and Petr Korba

Institute of Energy Systems and Fluid Engineering, School of Engineering, Zurich University of Applied Sciences (ZHAW), 8401 Winterthur, Switzerland; ramg@zhaw.ch (M.R.G.); korb@zhaw.ch (P.K.)
* Correspondence: kerd@zhaw.ch (S.K.); obus@zhaw.ch (A.O.)

Abstract: The increasing deployment of new technologies to contribute to the decarbonization of power systems is imposing new challenges in terms of system dynamics and stability. To deal with different operating and control issues in this sense, and support actual needs, advanced tools and solutions are required. Therefore, this paper presents a digital twin of a dynamic hardware emulator that can be used for controller hardware in the loop (CHIL) testing and is based on a small-scale laboratory system. To build the simulation model, the parameters of involved synchronous machines, excitation systems, prime movers and transmission lines have been identified and then compared to laboratory measurements to assess the accuracy of the digital twin. Static and dynamic accuracy have been investigated and an overall good accuracy can be shown with the help of quantification of errors. Furthermore, a case study is presented where the digital twin was used to design a controller to damp inter-area oscillations with the help of wide area measurements. This controller was then implemented and tested within the dynamic hardware emulator in the laboratory.

Keywords: digital twin; dynamic hardware emulator; parameter identification; power system dynamics; inter-area oscillations; wide area damping

Citation: Kellermüller, S.; Obushevs, A.; Ramirez Gonzalez, M.; Korba, P. Digital Twin Development of a Dynamic Hardware Emulator. *Energies* **2022**, *15*, 4547. https://doi.org/10.3390/en15134547

Academic Editor: Tek Tjing Lie

Received: 18 May 2022
Accepted: 17 June 2022
Published: 21 June 2022

1. Introduction

The continuous growth of the world's population, as well as the transition into a more sustainable behavior of the society that involves for example the shift to the E-mobility paradigm and the use of more environmentally friendly heating systems, increase the consumption of electric energy dramatically. Electric power systems are already the backbone of today's society, and the importance and value of their reliable operation will increase even more due to emerging trends. For example, the overall increasing penetration of new renewable energy sources (such as wind and solar power) is strongly affecting and changing system's dynamics, and consequent issues such as the reduction of the overall amount of inertia have to be timely addressed to keep the system stable [1]. In addition, since large renewable power plants are usually located far away from major load centers and power has to be transmitted over long distances, the system may be pushed to its transmission limits and different challenging problems related to low-damped inter-area oscillation modes can also appear [2]. Therefore, taking into account the aforementioned issues and the ever-increasing complexity of power systems, innovative concepts and advanced control structures are required to guarantee the stability of modern grids. In order to carry out lab research and have a hardware platform for the physical testing and evaluation of different power system solutions as close as possible to reality, a dynamic hardware emulator of an electrical power system (DHEPS) was built in [3]. Despite the enormous and valuable benefit in emulating power system dynamics through a DHEPS, the starting of the emulator can be very time-consuming at some point due to the sequential procedures to put in operation the different components involved, which may hinder its exploration under a broad range of operating scenarios and disturbances. Furthermore, some critical operating conditions may be difficult to achieve due to the high potential in damaging the hardware of the setup, which is costly. For this reason, a digital version of

the dynamic hardware emulator is needed. Here is where the concept of the Digital Twin (DT) come into picture. The general idea of a DT is to develop a digital counterpart of a corresponding entity in the physical world to replicate its characteristics and behaviors [4]. DTs can support not only a better understanding of the real-time performance of a given process under different operating scenarios, but also the implementation, testing, and pre-validation of advanced strategies without any risk to the physical object. According to [5], a formal definition of a DT can be given as follows:

> "A Digital Twin is the digital representation of a unique asset (product, machine, service, product service system or other intangible asset), that compromises its properties, condition and behaviour by means of models, information and data".

Some research works related to the application of DTs in the field of power systems can be already found in the literature. A comprehensive overview is given in [6–8]. Furthermore, information about online applications can be found in [9] and applications related to control rooms and substations is provided in [10–12]. However, unlike the mentioned publications available, the DT presented in this paper focuses on a scaled power system as a whole, including every single component which is physically installed. Based on the idea of a DT, the development of a simulation model for the unique dynamic hardware emulator in [3] is presented in this paper. In addition, to illustrate the application of the DT, a case study is included considering the damping improvement of inter-area oscillations using wide area measurements, where a control strategy is tested in a controller hardware in the loop setup and finally directly applied to the physical hardware emulator. More information about advanced laboratory testing can be found here [13]. The obtained digital replication provides better capabilities to analyze, understand and predict the operational behavior of the physical entity, as well as accelerate the design and evaluation of control strategies for dealing with different system stability issues. The scope of the paper is to demonstrate the process and gathered experience of developing a DT of the DHEPS and further show a possible application.

The remainder of the paper is organised as follows. In Section 2, the DHEPS is introduced and Section 3 refers to the modelling and parameter identification of different components, while in Section 4 the assembled DT is validated with measurements. Section 5 presents a case study, where the DT is used to test a controller and Section 6 is concluding the findings of the study.

2. Dynamic Hardware Emulator of a Power System

The DHEPS, visualised in Figure 1, is a scaled and slightly modified version of Kundur's two-area system [14] and, among other things, allows to perform lab-based hardware emulations of electromechanical oscillations in power grids. A single line diagram of the system is shown in Figure 2. In addition, primary and secondary frequency control functions are included, and there is also the possibility to separately change the inertia constant of each machine [3]. Therefore, equivalent inertia reductions can be carried out offline or online to emulate the frequency dynamics resulting from the integration of converter-interfaced generation and sudden islanded operating scenarios in large power systems [15]. Furthermore, each synchronous machine is equipped with a phasor measurement unit (PMU) that can be used for monitoring and control purposes. In general, the DHEPS represents a cyber–physical power system testbed for investigations such as:

- impact of low inertia sources (renewable energy sources (RES)/battery energy storage system (BESS)) on power system dynamics;
- equipment/protection behavior in case of high rate of change off Frequency (RoCoF);
- testing and validation of advanced wide area measurement, protection and control (WAMPAC) systems;
- validation of data-driven solutions including oscillation detection, classification and source allocation;

- de-risk grid control approaches and algorithms to achieve secure and resilient operation in normal and emergency grid conditions, including constraint violation avoidance;
- communication delays and packet loss in a 'riskfree' environment.

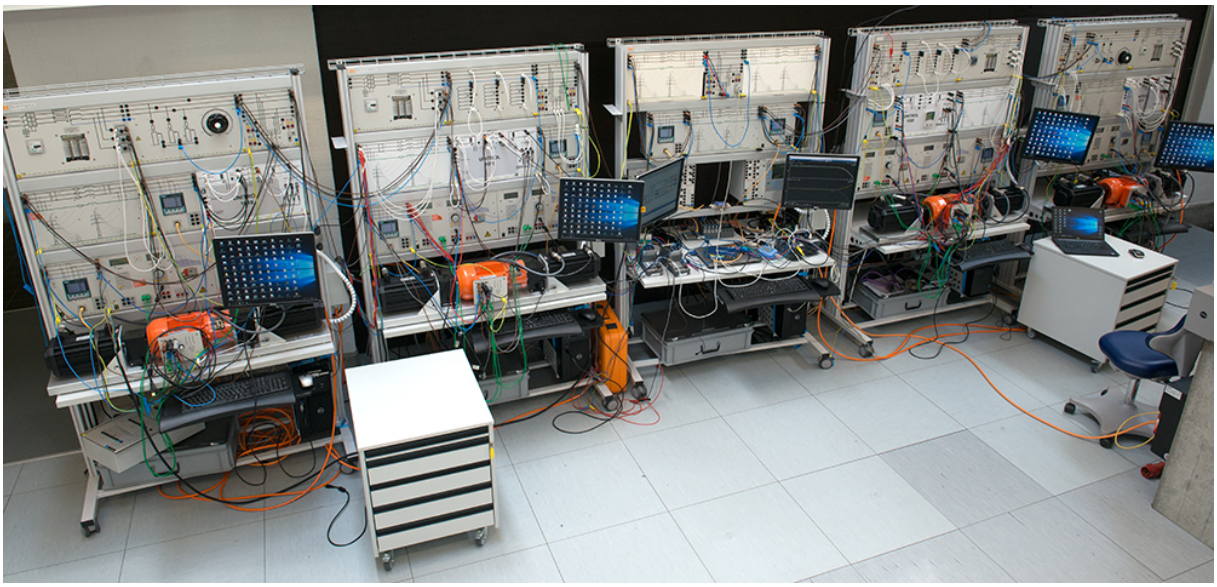

Figure 1. DHEPS in the REE-LAB of ZHAW.

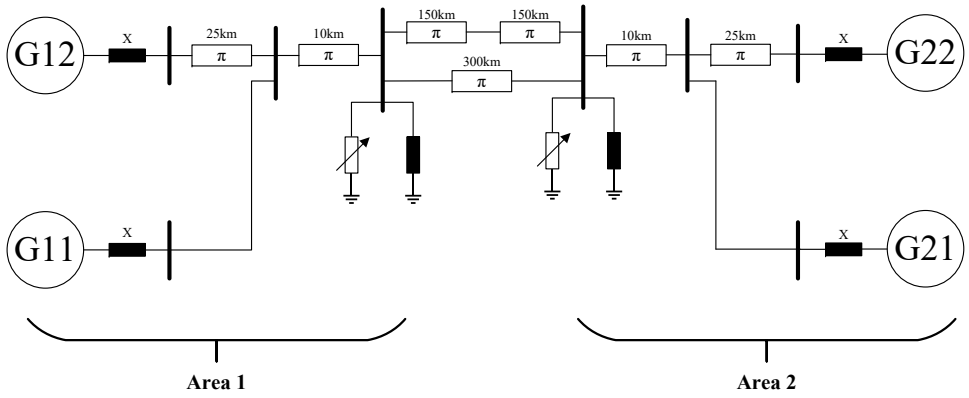

Figure 2. Single line diagram of the dynamic hardware emulator implemented in the lab according to [3] with its main components.

3. Modelling of Components

Power systems in general consists of many different components and control loops. The aim of this section is to briefly describe, how the parameters of the laboratory equipment were identified and which particular models were used in order to mirror the behaviour of the dynamic hardware emulator. In addition to the main components illustrated in Figure 2, such as synchronous machines, transmission lines and loads, this section provides also information about the modelling of the prime movers and the excitation systems, including automatic voltage regulators (AVRs).

3.1. Prime Mover

The synchronous generator is driven by a servo machine [16], which acts as a motor and converts electrical power into mechanical power. Furthermore, torque or speed of the servo machine can be controlled with a frequency converter. Since there are big discrepancies between the setpoint of the mechanical power of the servo motor and the electrical power measured at the terminals of the synchronous machine, a compensation

is needed for these losses. Generally, the losses could also have its origin on the electrical side of the synchronous machine, but since the resistance of the stator windings is rather small in this case, the major part of the losses are concentrated on the prime mover here. To be able to quantify those losses, an experiment was carried out where the generator is synchronized with the grid and the setpoint of the mechanical power is stair-wise increased while the active power at the terminals is measured. The results of this experiment are shown in Figure 3, where the black circles are the measured points and the solid red curve is the fitted linear function representing the characteristics. The approximation given by the linear function was then used for the conversion of the setpoint to the physically applied mechanical power on the shaft. It is important to mention, that the dynamics of the prime mover are neglected, since the control loops of the servo motor are very fast.

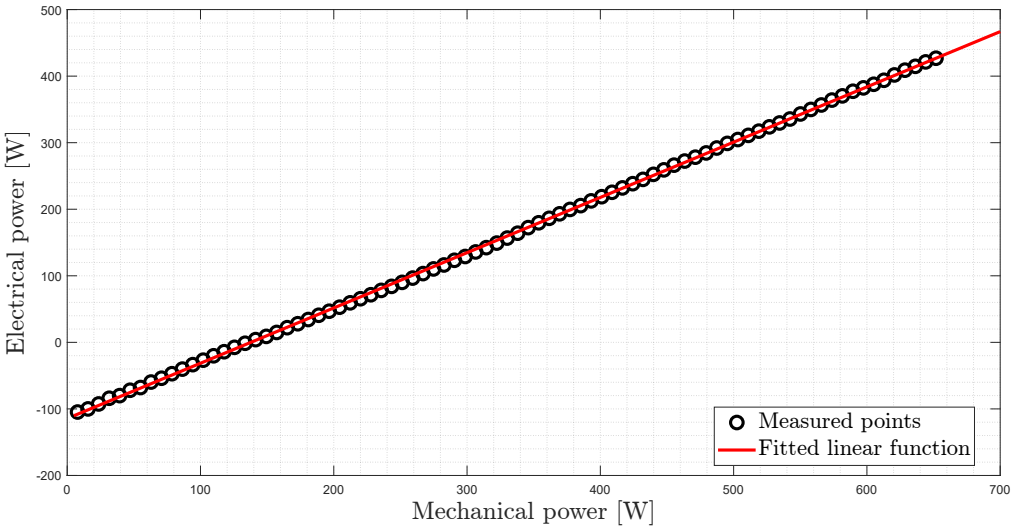

Figure 3. Measurement (circles) of the experiment and the corresponding fitted linear function.

3.2. Synchronous Machine

All the synchronous generators under consideration refer to a small scale round rotor machine with the ratings according to Table 1.

Table 1. Ratings of the laboratory synchronous machine according to the plate mounted on the machine.

Rating	Value
Rated voltage (Y/Δ)	400/230 V
Rated current	1.5/2.6 A
Synchronous speed	1500 rpm
Rated frequency	50 Hz
Rated power	800 VA

3.2.1. Saturation Characteristics

In general, the magnetic circuit of a synchronous machine consisting of the iron path and the air gap starts saturating at some point, which means that the relationship between the excitation voltage/current and the induced voltage of the machine is not linear anymore. Therefore, in order to quantify this saturation, the so called open circuit characteristics is measured, where the generator stator is open-circuited and the excitation current is increased step by step. The resulting characteristic and the saturation effect are visualised in Figure 4 where, in addition to the saturation characteristics, the air gap line is also plotted, which represents the behaviour for the case of no saturation. By using a polynomial function of order five, the measured results can be approximated as illustrated in Figure 4. Since the saturation characteristics were measured on no load conditions, the

corresponding representation for normal load conditions may differ. However, since this is often the only available information, it can still be used for the case where the machine is loaded, according to [17].

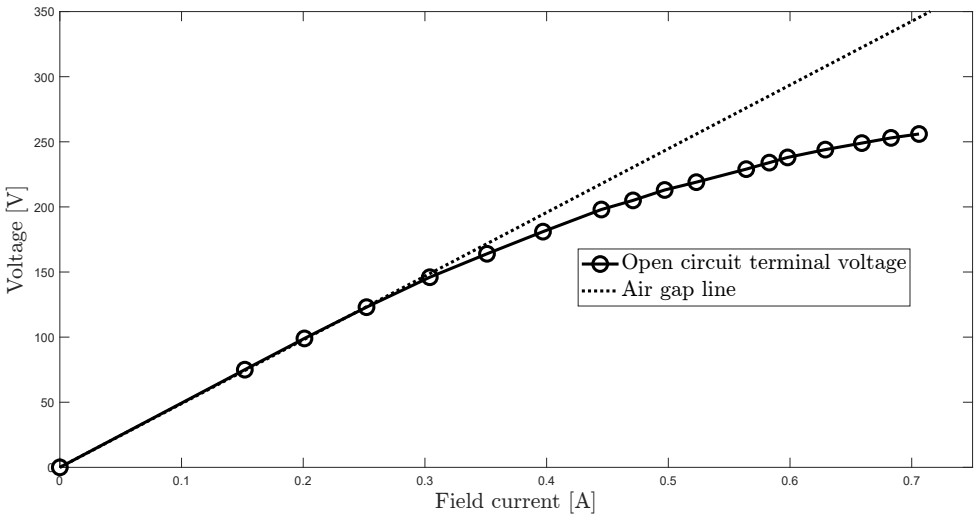

Figure 4. Open circuit characteristics and air gap line of the synchronous machine under consideration.

3.2.2. Electrical Parameters

A common way to express the parameters of synchronous machines is to use the dq-reference frame, where Park's transformation is applied to change the reference frame. Furthermore, the parameters are stated with respect to steady state, transient and subtransient conditions, and thus the parameters shown in Table 2 are generally considered [17]:

Table 2. Generic parameters of a synchronous machine in dq-reference frame.

***d*-axis**	***q*-axis**
X_d: synchronous reactance	X_q: synchronous reactance
X'_d: transient reactance	X'_q: transient reactance
X''_d: subtransient reactance	X''_q: subtransient reactance
T'_{do}: transient open circuit time constant	T'_{qo}: transient open circuit time constant
T''_{do}: subtransient open circuit time constant	T''_{qo}: subtransient open circuit time constant

In order to be able to identify the information indicated in Table 2, several tests were accomplished according to the IEEE Guide for Test Procedures for Synchronous Machines Including Acceptance and Performance Testing and Parameter Determination for Dynamic Analysis [18].

First of all, two test procedures were applied in order to find the *d*-axis parameters, namely the load rejection test and the voltage recovery test according to [18]. In the case of the load rejection test, the synchronous generator is initially synchronized with the grid and it is important to make sure that no active power is delivered and that the generator is under- or overexcited. This is crucial because then the entire current is flowing in the *d*-axis and thus the *d*-axis parameters can be estimated. The second step is to open the circuit breaker between generator and grid and record the transient voltage at the terminals. Since it is important to keep a constant excitation voltage during the test, the excitation voltage can be recorded for verification. The received transient voltage response can be approximated with the following equation [18]:

$$\begin{aligned} E(t) &= E_0 - \left[X_d - \left(X_d - X'_d\right) e^{\frac{-t}{T'_{do}}} - \left(X'_d - X''_d\right) e^{\frac{-t}{T''_{do}}} \right] I_0 \\ &= E_{q\infty} + E'_q(t) + E''_q(t) \end{aligned} \tag{1}$$

where E_0 is the pre event RMS voltage, I_0 is the pre event RMS current, and $E''_q(t)$, $E'_q(t)$ and $E_{q\infty}$ are used to denote the subtransient, transient and steady state components, respectively.

The second test performed to estimate the d-axis parameters is called voltage recovery test [18]. The machine runs initially at rated speed and the stator windings are short circuited while the excitation current is bigger than zero and a short circuit current starts flowing. Then the circuit breaker is opened and the transient terminal voltage is recorded. Again, the excitation voltage should be kept constant during the test. The transient voltage can be approximated in this case according to:

$$\begin{aligned} E(t) &= \left[X_d - (X_d - X'_d)e^{\frac{-t}{T'_{do}}} - (X'_d - X''_d)e^{\frac{-t}{T''_{do}}} \right] I_0 \\ &= E_{\Delta\infty} + E'_\Delta(t) + E''_\Delta(t) \end{aligned} \tag{2}$$

where I_0 is the pre event RMS armature current. The voltage response can also be represented by three characteristic states, as indicated by Equation (2).

Finally, to receive the d-axis parameters according to Table 2, Equations (1) and (2) needs to be fitted to the collected measurements. Both equations share the same parameters and thus a multi curve fitting algorithm called Marquardt-Fit-Method [19] has been used and implemented in Matlab for this purpose. It is important to mention at this point, that the different tests need to be done at approximately the same level of saturation in order to receive meaningful solutions.

Unfortunately, it was not possible to identify the subtransient state associated with $E''_\Delta(t)$ and $E''_q(t)$ since the subtransient time constant is too short to be captured with RMS measurements taken every 0.01 seconds. The reason for this was considered to be in the fact that the machines are very small. Due to this, Equations (1) and (2) were simplified as follows:

$$\begin{aligned} E(t) &= E_0 - \left[X_d - (X_d - X'_d)e^{\frac{-t}{T'_{do}}} \right] I_0 \\ &= E_{q\infty} + E'_q(t) \end{aligned} \tag{3}$$

$$\begin{aligned} E(t) &= \left[X_d - (X_d - X'_d)e^{\frac{-t}{T'_{do}}} \right] I_0 \\ &= E_{\Delta\infty} + E'_\Delta(t) \end{aligned} \tag{4}$$

Based on Equations (3) and (4) the curve fitting algorithm provided the results depicted in Figure 5, where each test has been repeated twice. The algorithm works well and the fitted functions with the shared parameters fits nicely the recorded measurements in the laboratory. The obtained numerical values are given in Table 3.

Since there are not many test procedures in [18] regarding the q-axis parameters, it is difficult to perform similar tests as for the d-axis. Furthermore, most likely the subtransient state can also not be captured at all and if it is assumed that there is no winding in the q-axis representing the rotor body the transient parameters of the q-axis are not needed [17]. Finally, since the the involved machine has a round rotor, it can be assumed that $X_d = X_q$ [17]. Due to different issues in determining the parameters for the involved synchronous machines according to detailed representations, a second order model was adopted in this work.

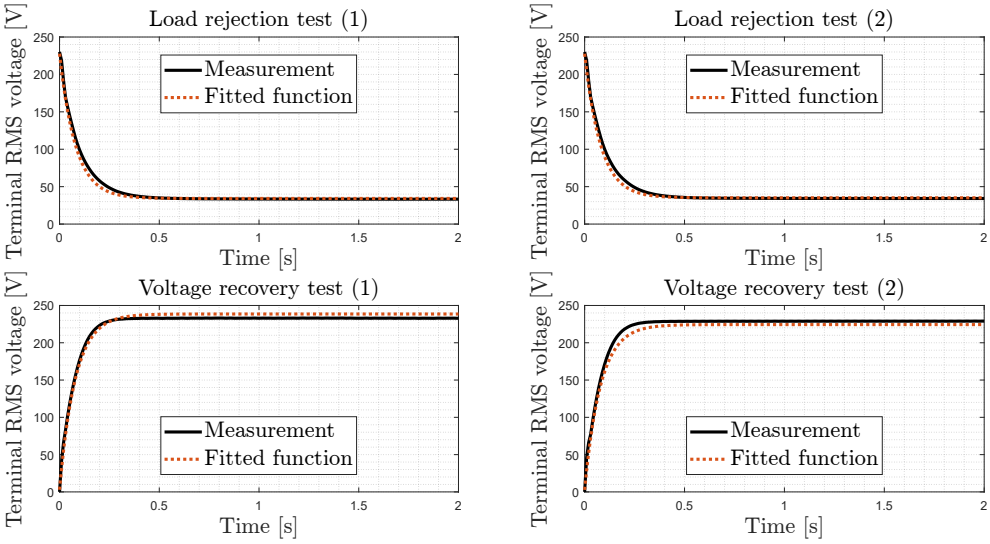

Figure 5. Top row: Measurement (solid line) and fitted function (dashed red line) of the load rejection test where the same test has been repeated twice. Bottom row: Measurement (solid line) and fitted function (dashed red line) of the voltage recovery test where the same test has been repeated twice.

Table 3. Estimated electrical parameters *d*-axis.

Parameter	Value
X_d	322.8 Ω
X'_d	3.9 Ω
T'_{do}	0.0798 s

3.2.3. Mechanical Parameters

The structure of the mechanical part of the second order model of a synchronous machine is described with the following equations:

$$\begin{aligned} 2H\Delta\dot{\omega} &= T_m - T_e - K_d\Delta\omega \\ \Delta\dot{\omega} &= \omega - \omega_0 = \frac{d\delta}{dt} \end{aligned} \tag{5}$$

where T_m is the mechanical torque in p.u., T_e is the electrical torque in p.u., H is the inertia constant in s, ω is the speed of the rotor in p.u., and K_d is the damping factor. Thus, the unknown mechanical parameters are the inertia constant H and the damping factor K_d. To gain a chance to identify those two parameters, the idea was to provoke electro mechanical oscillations in the laboratory and then apply the same configuration in a simulation environment and compare and fit the results. An easy way to gain electro mechanical oscillations is to apply a step in the mechanical power while the machine is synchronized with the grid. The signal to be monitored is the active power of the machine fed to the grid. Since the moment of inertia attached to the machines can be varied with the help of a software [3] (the range goes from 0 to 2500, but is is not known in advance which value corresponds to which moment of inertia), a series of experiments need to be done in order to cover the whole range applicable in the laboratory. To finally gain the parameters H and K_d, the same step in the torque was applied using a simulation model in Simulink, and then the active power of the simulation and the active power of the measurement were compared and the parameters to find adjusted with the help of the parameter estimation tool in Simulink. Figure 6a shows an example of the fit for the active power dynamics after using the parameter estimation tool, and Figure 6b displays the inertia constant H in seconds and the damping coefficient K_d in pu for different values (100 to 1200 in steps of 100) set in the software.

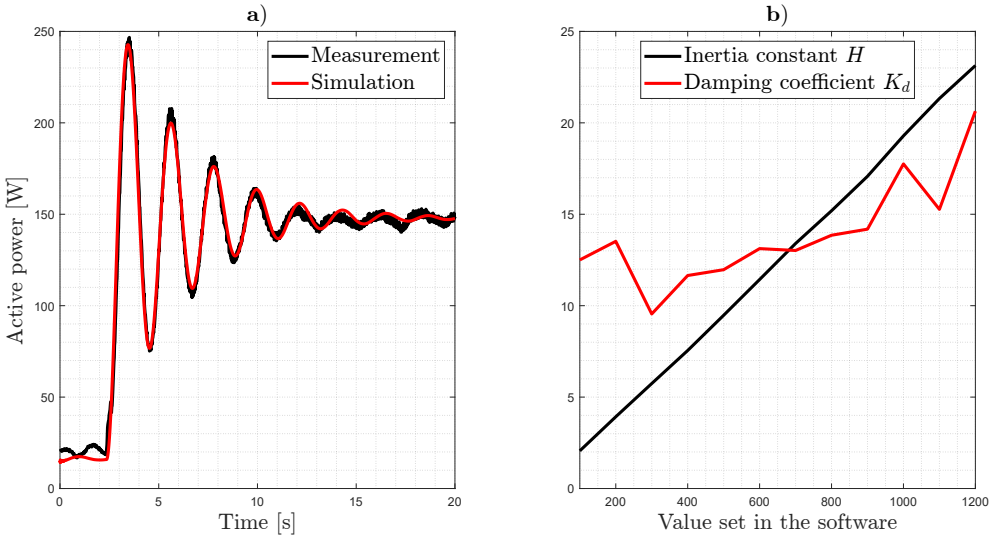

Figure 6. (**a**): Active power of the simulation (red) and measured active power (black) after convergence of the parameter estimation tool for a value of 600 defined in the software. (**b**): Inertia constant H in seconds and damping coefficient K_d in pu depending on the value set in the software.

3.3. Excitation System and AVR

The excitation systems used in the laboratory are Unitrol 1010/1020 from the manufacturer ABB [20]. Unfortunately, the structure and type of the AVR is not known and thus a relatively simple model for the excitation system was considered here, such as the IEEE AC4A type illustrated in Figure 7, where V_C is terminal voltage to be controlled,V_{ref} is the reference voltage to be achieved, V_{PSS} is an additional term dedicated to the output of a power system stabilizer (PSS), and E_{fd} is the field voltage applied to the machine. Based on this model, the parameters to be identified are the time constants T_R, T_B, T_C, T_A and the gain K_A.

To estimate these parameters, the experiment described next has been carried out in the lab. With the generator running at synchronous speed (no load) and the Unitrol connected with an active AVR, a step change of 2.5% in the reference voltage is applied and the terminal voltage as well as the field voltage are measured with the built-in oscilloscope of the Unitrol. The estimation process was done with the parameter estimator tool from Matlab Simulink where the lab experiment was replicated. Moreover, the reference voltage and the measured terminal voltage served as inputs to the simulation model of the excitation system and the signals to be compared were the measured and simulated field voltages.

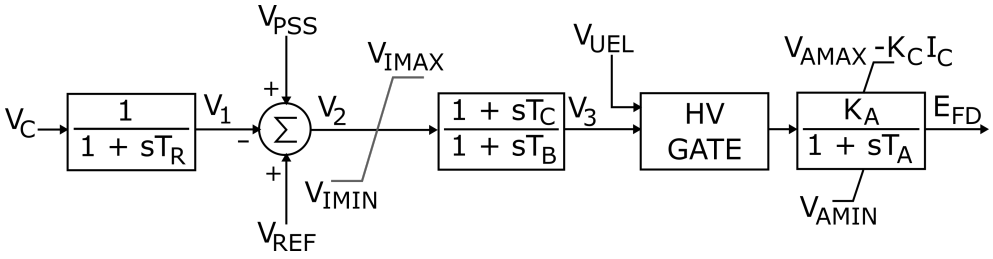

Figure 7. Block diagram of the excitation system type IEEE AC4A [21].

Figure 8 displays the obtained results after the identification process, where the measured field voltage and the simulated field voltage are drawn in black and red, respectively, and the AVR reference voltage is drawn in blue. Moreover, the corresponding measured terminal voltage is colored in green. In this case, the numerical values achieved for the estimated parameters are given in Table 4.

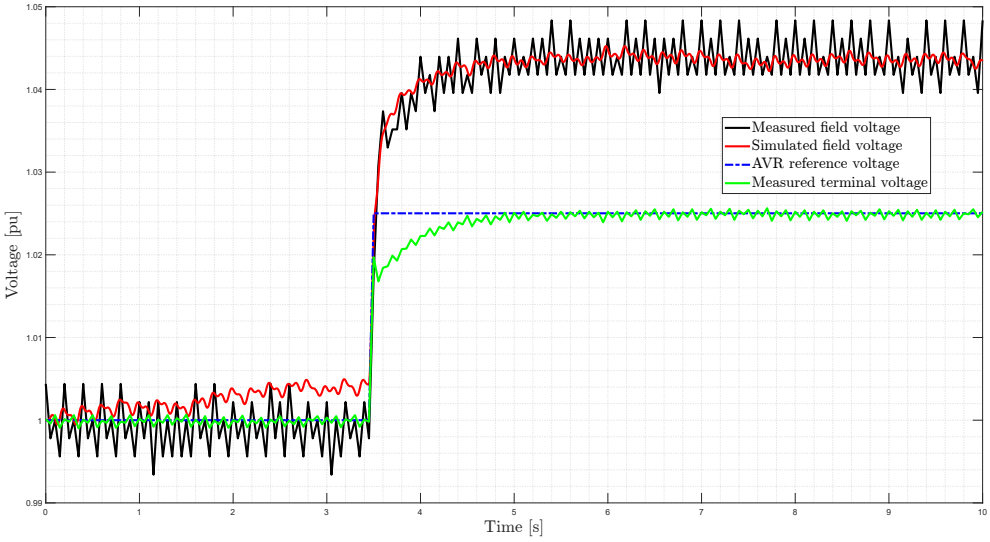

Figure 8. Final result after identification process where the dashed blue line indicates the step in the reference voltage and the black and red line the measured and simulated field voltage.

Table 4. Estimated parameters of the excitation system IEEE AC4A.

Parameter	Value
T_R	0.01
T_B	32.6876
T_C	0.3408
T_A	0.0347
K_A	310

3.4. Transmission Lines

Since π-type equivalents are used in the lab in order to replicate the behaviour of transmission lines, π equivalents were also considered which are illustrated in Figure 9. Despite that the values of the involved capacitances, inductances and resistances are given by the manufacturer, they are often not very precise and thus the resistances and the inductances were determined from measurements with an LCR metering device. Moreover only the series elements of the resistance and inductance have been taken into account, and no mutual effects were considered regarding these elements.

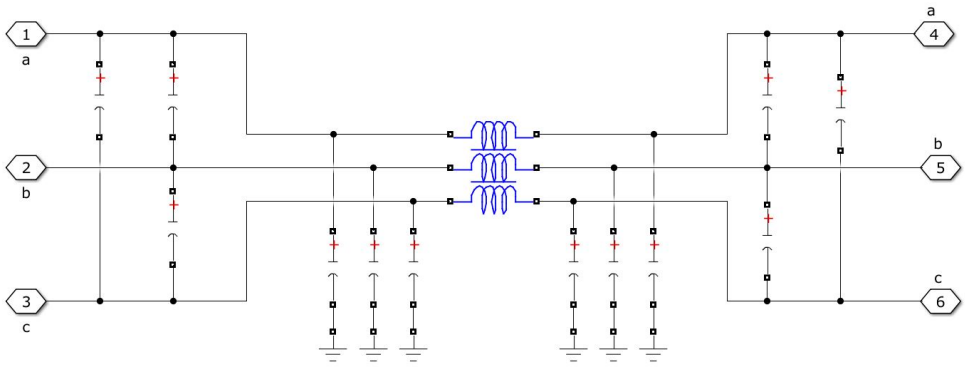

Figure 9. Representation of the π-type transmission line model used in Simulink.

4. Digital Twin Validation

With the help of the modelled components described in Section 3, a complete model has been assembled to represent the topology shown in Figure 2. The validation of the model

was divided into purely static conditions and dynamic conditions during a disturbance, as described next.

4.1. Static Conditions

Several simulations and measurements for steady state conditions under different operating points were performed. The operating points differ from each other in terms of the loading of the synchronous machines. Every machine is equipped with a PMU and thus the active power P, reactive power Q, terminal voltage U, frequency f and the phase current I were measured and then compared to the values generated with the digital twin. Figure 10 displays the resulting errors in % according to the loading of the machine, where the base values can be found in Table 1. Every point in Figure 10 represents the error of the specific variable for a particular synchronous machine, where colored dots are used to identify a given and corresponding operating point in plots (a–e). Special attention has been given to the current errors, because one important issue of the dynamic hardware emulator is the current limitation of 1.2 A through the 10km transmission lines [3]. In order to not exceed this limit while applying certain operating conditions, a precise simulation is crucial. It can be seen from plots (a–e) that the errors are in general within a few percent and thus within an acceptable and satisfactory range.

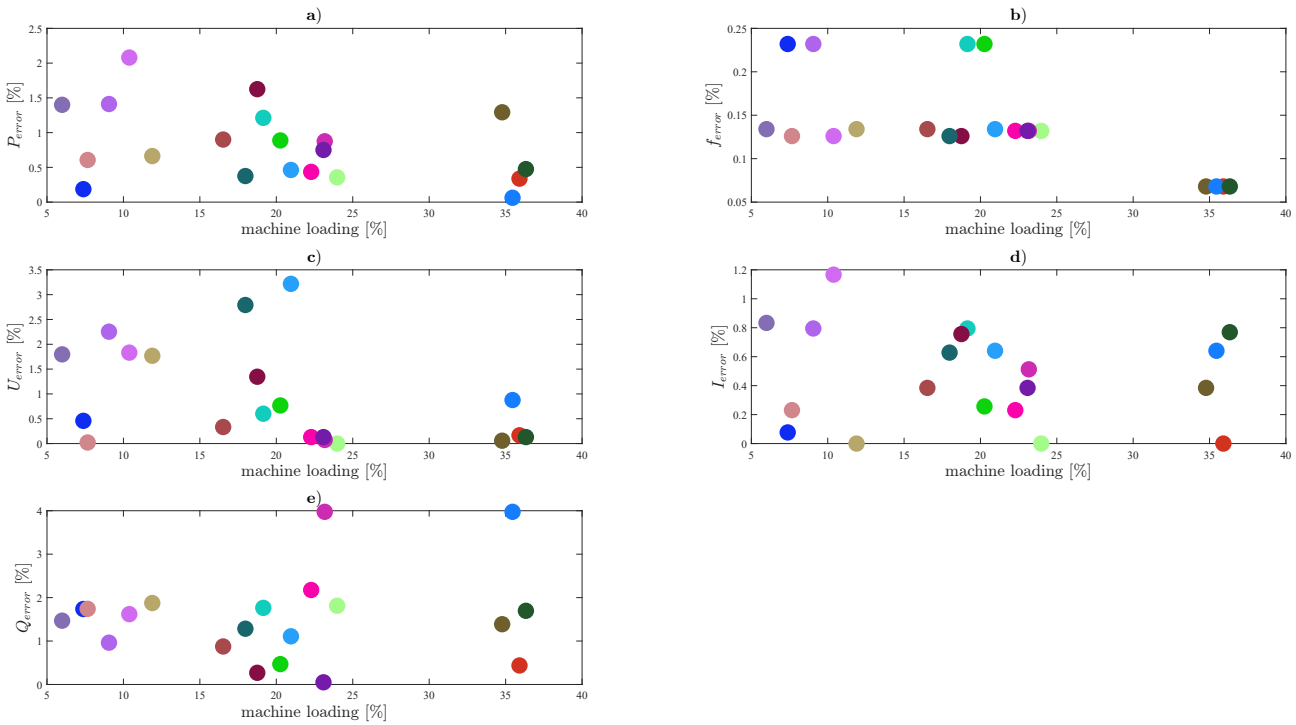

Figure 10. (**a–e**) Errors of the measured signals compared to the simulation output in % depending on the loading of the machine.

4.2. Dynamic Conditions

In order to assess the dynamic behaviour provided by the simulation model, a sudden step increase of the ohmic load in area 1 (see Figure 2) was considered. Then, PMU measurements obtained from the hardware emulator and the corresponding dynamics achieved by the simulation model after the same event were compared. For this experiment, secondary frequency control was disabled, but the primary frequency control was active. The obtained results are illustrated in Figure 11, where plots are organized in a matrix form such that each column is associated with a given synchronous machine, and every row portrays the response of a particular electrical quantity. In addition, behaviour related to the simulation model can be identified by the red curves, and the one from the hardware emulator is given by the black curves. In order to have a quantitative measure for the

evaluation of these results, the resultant errors were estimated according to the root mean square errors (RMSE) metric, and are provided in Table 5. As it can be noticed, the biggest errors are associated with the reactive power Q, which can be attributed mainly to differences between the AVR used in the digital twin and the real one incorporated into the Unitrols 1010/1020 of the hardware emulator, as well as some other differences in the inductive/capacitive effects of the components involved. In general, as it can be observed from Figure 11, the terminal voltage fits well and the deviations in the frequency are relatively small. In addition, it can be noticed that the active power correlates well with the current. Although it is clear that in this case the corresponding dynamic behaviours do not match exactly, the steady state values after the disturbance tend to be relatively close.

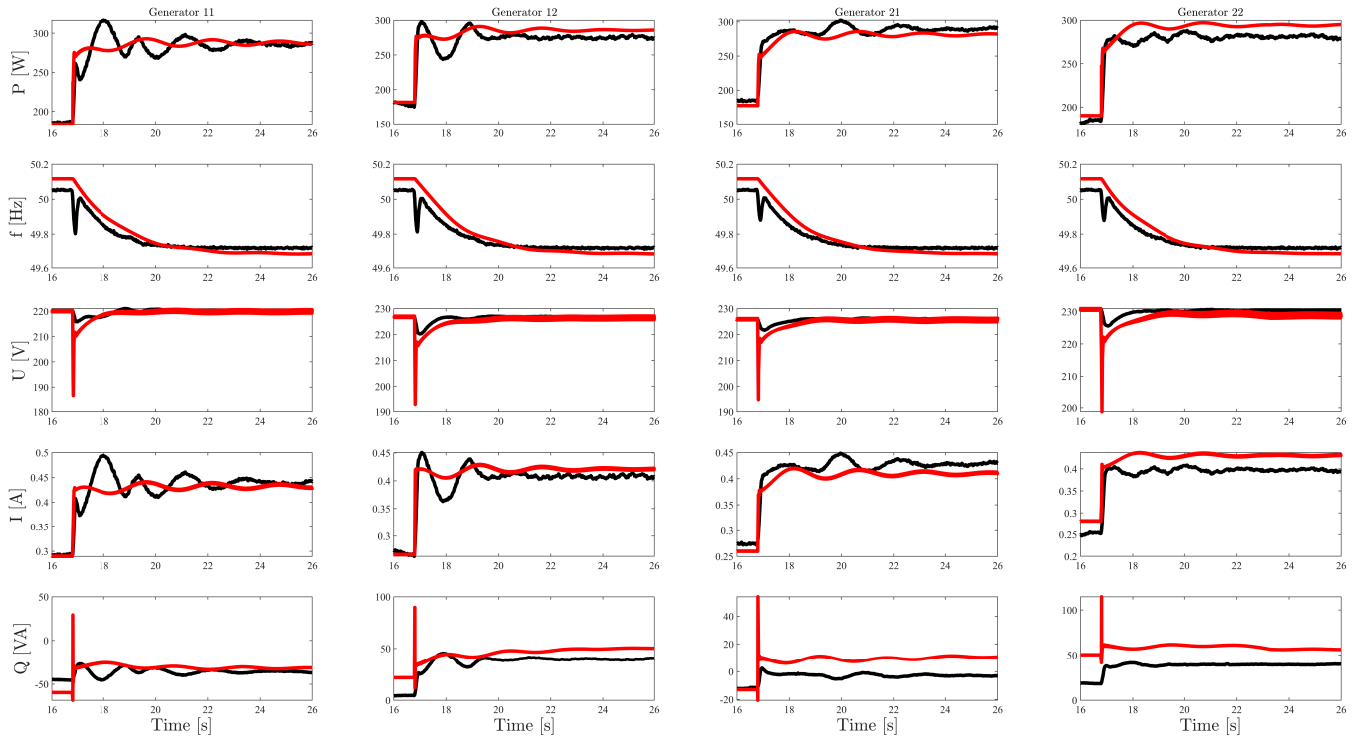

Figure 11. Measured (black) and simulated (red) signals (active Power P, frequency f, terminal voltage U, phase current I and the reactive power Q) of the the four synchronous machines after the event.

Table 5. RMSE in % of the signals displayed in Figure 11.

	Generator 11	Generator 12	Generator 21	Generator 22
RMSE P in %	0.96	0.56	1.00	1.28
RMSE f in %	0.05	0.05	0.05	0.05
RMSE U in %	0.23	0.24	0.44	0.02
RMSE I in %	0.35	0.31	1.21	0.65
RMSE Q in %	1.61	1.07	2.99	1.00

5. Case Study Involving the Digital Twin

The developed digital representation of the dynamic hardware emulator can be used for a wide range of applications. For illustrative purposes, a case study is considered here where a wide-area damping controller (WADC) strategy, together with a conventional power system stabilizer (PSS), are designed, implemented and tested to damp the electromechanical oscillations of the system. To successfully accomplish this, a two stage approach has been pursued here. In in the first stage the digital twin is used within a controller hardware in the loop (CHIL) setup with the considered digital control algorithm

programmed and implemented on a micro computer for pre evaluation purposes. In the second stage the digital controller is connected and integrated into the dynamic hardware emulator, and tested under a real and practical environment. In this way, the digital twin can be used to design, explore and validate the response of the given control strategy in a HIL setup before moving it to the dynamic hardware emulator.

5.1. Controller Implementation in the CHIL Setup and Results

The CHIL setup considered here consists of an OPAL-RT real time simulator, two National Instruments cRIO devices used as Phasor Measurement Units (PMU) [22], and a Raspberry Pi micro computer that is used as the digital controller. Furthermore, the Raspberry Pi is equipped with an expansion board in order to be able to generate analog output signals. Figure 12 illustrates the CHIL setup, where the digital twin has been implemented in the OPAL-RT real time simulator and the three phase terminal voltages of the two considered machines are obtained through PMUs. Moreover, the Raspberry Pi reads the electrical frequency values through a python script [23] and proccesses them according to the control structure. After processing the inputs, the Raspberry Pi provides the controller's output signals to the OPAL-RT within a range of 0 V to 5 V. The structure of the conventional PSS used in the damping control strategy is shown in Figure 13, which consists of a washout filter, a proportional gain, two lead/lag elements and a limiter at the output. Moreover, a first order lowpass filter is used to filter the frequency deviation $\Delta\omega$. For the WADC only a proportional gain has been considered here, which acts on the frequency deviation between the two areas as displayed in Figure 12. The machines involved in the control scheme are identified as Generator 11 and Generator 21.

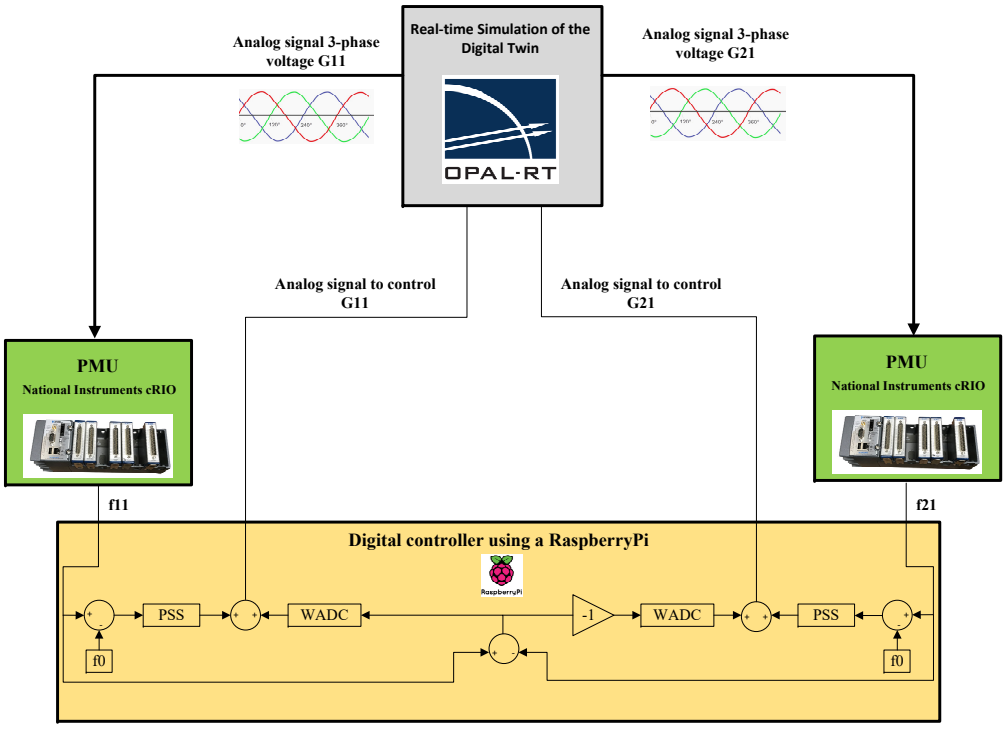

Figure 12. Schematic drawing of the HIL setup including the real time simulator, PMUs and the digital controller.

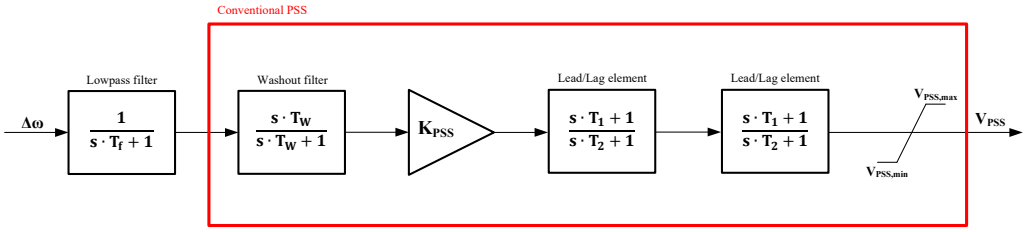

Figure 13. Conventional PSS (red frame) and the corresponding elements plus a lowpass filter to filter the input signal.

Three cases have been tested and compared to each other: first of all without any additional control loop, then with the active PSS only, and lastly with the PSS and the WADC. The frequency after the trip of one of the tie lines is shown in Figure 14, where the black curve indicates the case without any additional control loop, the red curve shows the PSS only case and the blue curve the combination of PSS and WADC. It can be seen that both the PSS only case and the combination of PSS and WADC can improve the damping of the system's electromechanical oscillations. Since the control strategy was implemented on generators 11/21, the combined effect of the WADC and the PSS on these machines is relatively better than in the other two machines. In addition to the results shown in Figure 14, the frequency deviation between the areas is plotted in Figure 15 to further demonstrate the effectiveness of the implemented controllers. It is worth mentioning here that the control strategy was empirically tuned, but a better and advanced approach will be applied in related future research.

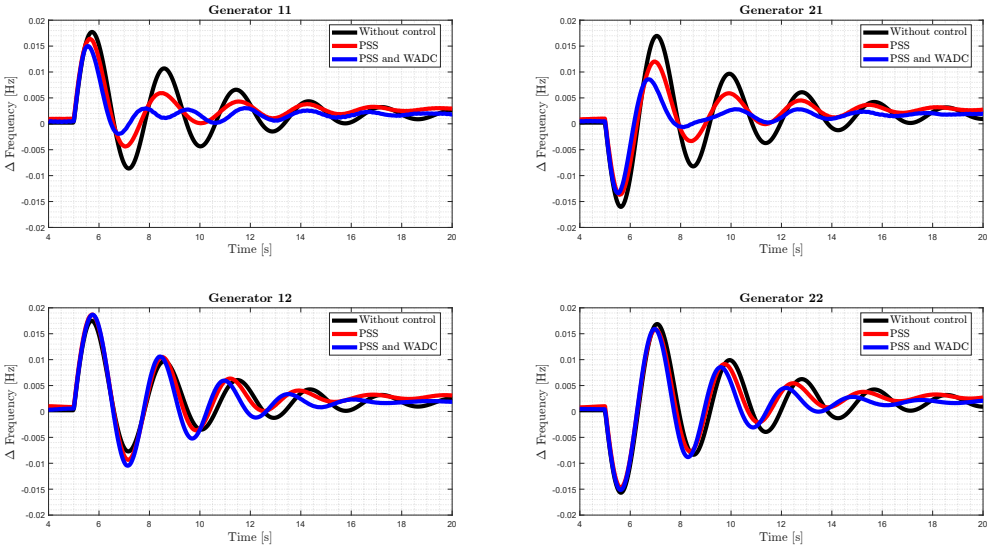

Figure 14. Comparison of the frequency deviations in the CHIL setup of the three cases (without control, PSS only, PSS and WADC) after applying the same event.

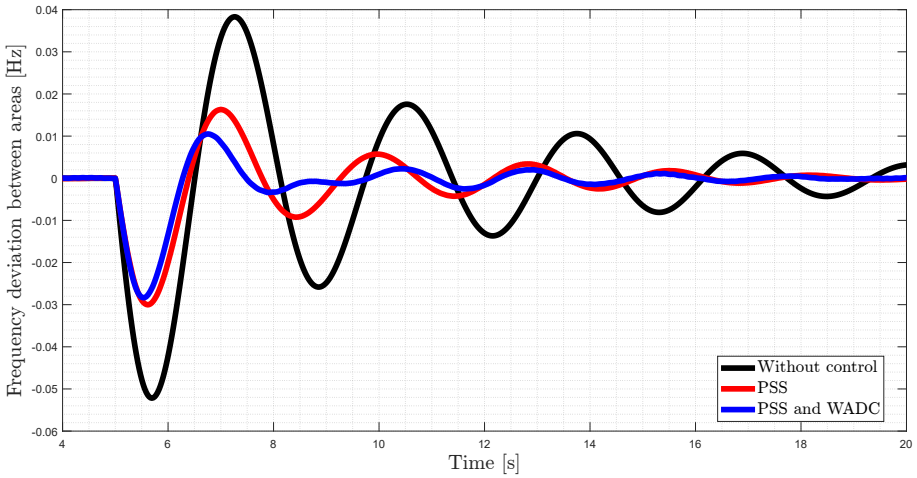

Figure 15. Frequency deviation between area 1 and area 2 for the three cases (without control, PSS only, PSS and WADC) after the tie line trip within the CHIL setup.

5.2. Controller Implementation in the Dynamic Hardware Emulator Setup and Results

After the evaluation in the CHIL setup, the control scheme is implemented to directly interact with the dynamic hardware emulator, according to the configuration shown in Figure 16. In this case, instead of simulating the digital twin on the OPAL-RT, the control scheme under concern is connected to the dynamic hardware emulator, where corresponding control signals are passed to real Unitrol excitation systems. Furthermore, the same type of PMUs (National Instruments cRIO) are used and the same generators as in the CHIL setup are beeing controlled. The applied event is again a line trip of one of the tie lines, when approximately 300W active power is being transferred from area 1 to area 2. Due to amplification issues of the high frequency noise in the frequency signal, the structure of the PSS had to be changed slightly and thus only one lead/lag element was considered, whereas the structure of the WADC remains unchanged.

Again the same three cases (without additional control loop, conventional PSS only and PSS combined with WADC) have been investigated and compared with each other. It can be inferred from this figure that the damping of the inter-area mode is improved with the help of the PSS as well as with the combination of the PSS an the WADC. Important to mention at this point is that the very sharp change of the frequency just after the event (see Figure 17) does not refer to a action of the controller. This phenomena can also be observed in the case where no additional controller is used and has to do with a measurement issue of the PMUs, which is investigated in [24]. It is removed with the help of a filter, which limits the maximum value of the derivative and thus prevents any problems while processing the signal in the controller.

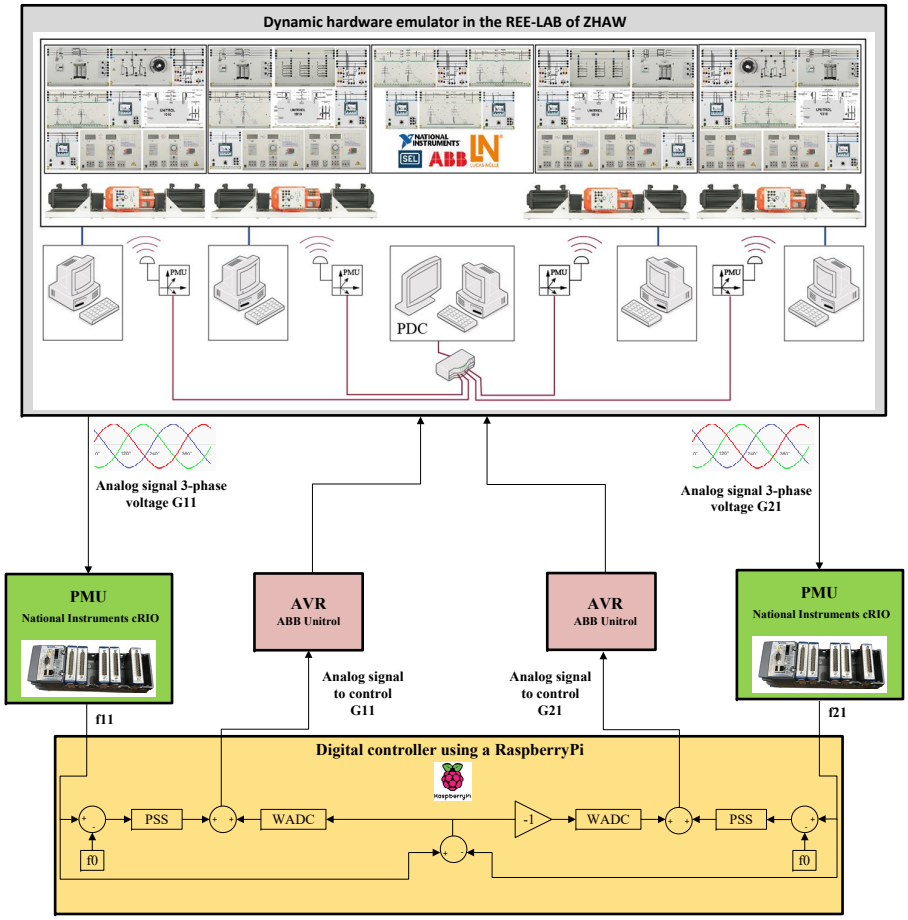

Figure 16. Schematic drawing of the dynamic hardware emulator setup including the PMUs, the digital controller and the ABB Unitrol.

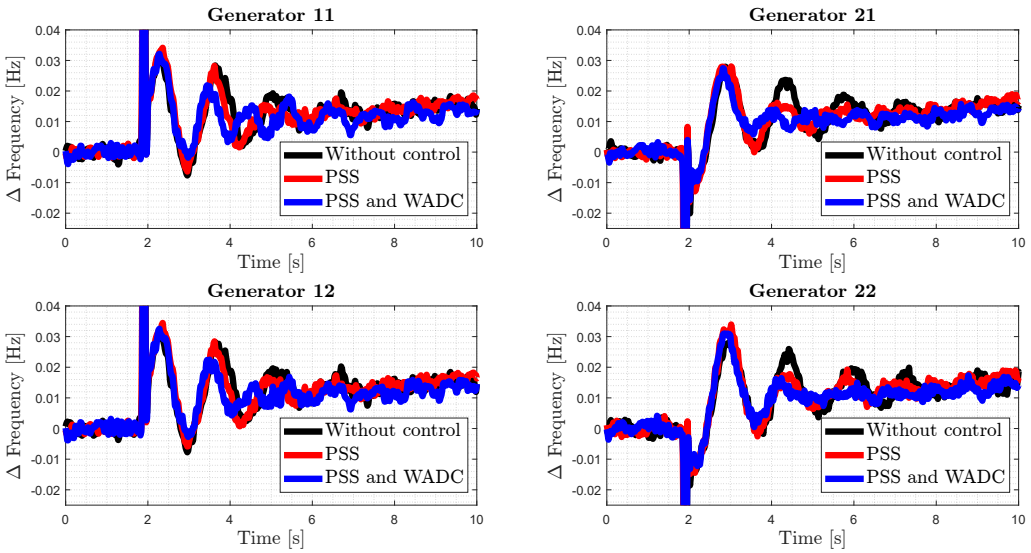

Figure 17. Frequency deviation with respect to the pre-fault value for the three cases (without control, PSS only, PSS and WADC) after the tie line trip within the setup with the dynamic hardware emulator.

In order to quantitatively evaluate the responses in Figure 18, a performance index was computed according to the following expression:

$$S = \sum_{t=0}^{t_{end}} |f(t) - f(t-1)| \cdot t \tag{6}$$

where $f(t)$ refers to the frequency deviation at time instant t, $f(t-1)$ refers to the the frequency deviation at time instant $t-1$ and t is the time, which starts counting at the moment the disturbance happened. The absolute difference of two consecutive points in the frequency deviation signal is multiplied with the corresponding time and summed up, whereas the multiplication with the time t has the effect, that deviations of two consecutive points at a relatively long time after the disturbance are weighted strongly and thus poor damping is reflected with a high performance index. Results obtained in this way are given in Table 6, where it can be clearly seen that the WADC strategy is able to provide a better damping performance. Note that the indexes are normalized in order to gain a value of 1 for the case without control.

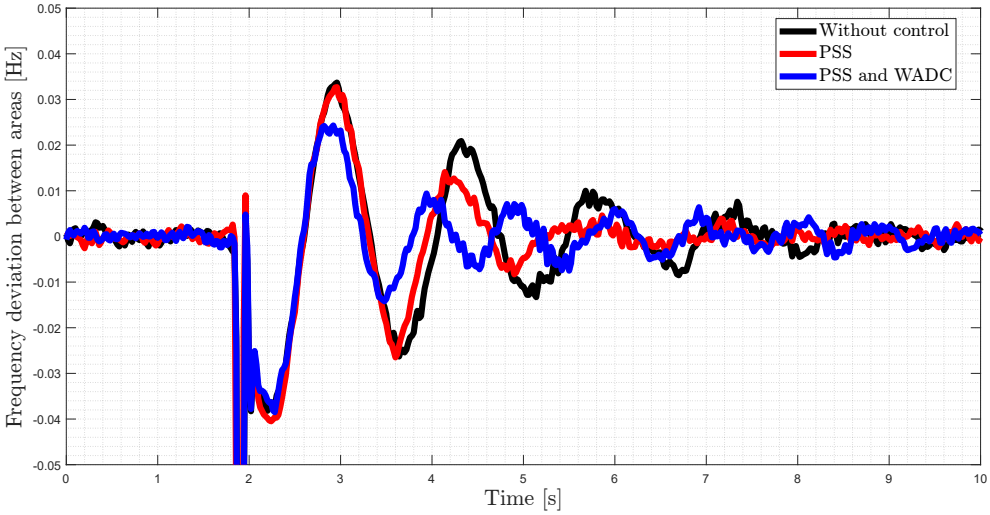

Figure 18. Frequency deviation between area 1 and area 2 for the three cases (without control, PSS only, PSS and WADC) after the tie line trip within the setup with the dynamic hardware emulator.

Table 6. Normalized performance index of the three cases (without control, PSS only, PSS and WADC) for the frequency deviation between the areas within the dynamic hardware emulator setup.

	Performance Index
Without control	1
PSS only	0.86
PSS / WADC	0.82

6. Conclusions

This paper presents a digital twin of the dynamic hardware emulator located in the laboratory of ZHAW and, in addition, a case study of the digital twin in order to damp inter area oscillations with a wide area damping controller. During the creation of the digital twin, the following challenges and gaps were identified:

- It was challenging to identify the parameters of many components, since a lot of measurements need to be done in the laboratory.
- Merging components together in a simulation environment does not always lead to a stable solution and thus self-tuning of the model is necessary.

- Static accuracy of the digital twin is satisfactory, although the reactive power was for some machines not very accurate and thus further improvements are needed, which will be addressed in further research.
- Due to the fact that there is a bottleneck in terms of current limitation of the 10 km transmission lines of 1.2 A, it can be observed that in general the machines were operated with loadings less than 40%. As per this aspect, it is important to mention here that the cumulated current of the machines in the same area should not exceed 1.2 A to avoid damaging the equipment.
- In terms of dynamics, the errors are in an acceptable range, even if there are at some specific points significant differences. Therefore, it can be concluded that the digital twin is not perfect and there is room for improvement. However, it is believed that its actual state (according to the results of this work) represents a good starting progress for the development of an enhanced version in the near future.
- Finally, the case study demonstrates the benefit of having a digital twin, which among other things allowed the evaluation and testing of the involved control scheme in a real-time environment, where nothing can be damaged.

Future research activities are planned to migrate the digital twin into a more power system oriented software such as DigSilent Power Factory since it can offer a lot more possibilities regarding analysis of the model. Furthermore, continuous improvement of the DT is necessary to gain a more accurate representation of the dynamic hardware emulator, for example a more detailed model of the excitation system and the synchronous machines. In addition, more complex controller structures in terms of damping inter area oscillations can be implemented and tested, for example those mentioned in [25]. Another issue, which can be investigated is the loss of time synchronization signal on PMU based applications and its impact on the stability similar as in [26].

Author Contributions: Conceptualization, methodology, software, validation, and formal analysis, S.K., A.O. and M.R.G.; investigation, writing—original draft preparation, visualization, S.K.; writing—review and editing, A.O. and M.R.G.; supervision, project administration and funding acquisition, P.K. All authors have read and agreed to the published version of the manuscript.

Funding: Open access funding provided by ZHAW Zurich University of Applied Sciences.

Institutional Review Board Statement: Not applicable.

Informed Consent Statement: Not applicable.

Data Availability Statement: Not applicable.

Acknowledgments: Special thanks to the Institute of Energy Systems and Fluid Engineering at ZHAW for the access to the REE-LAB and to the Swiss Federal Office of Energy (SFOE) under «Smart Grid International Research Facility Network» (SIRFN) co-operative programme on smart grids (ISGAN) (Grant Agreement No. SI/501524-01) for the support.

Conflicts of Interest: The authors declare no conflict of interest.

Abbreviations

The following abbreviations are used in this manuscript:

HIL	Hardware in the loop
DHEPS	Dynamic harware emulator of an electric power system
PMU	Phasor measurement unit
DT	Digital twin
AVR	Automtic voltage regulator
RMS	Root mean square
PSS	Power system stabilizer
RMSE	Root mean square error
WADC	Wide area damping controller
CHIL	Controller hardware in the loop

REE-LAB	Renewable Electrical Energy Laboratory
WAMPAC	Wide Area Measurement, Protection and Control
RES	Renewable energy source
BESS	Battery energy storage system

References

1. Fernández-Guillamón, A.; Gómez-Lázarob, E.; Muljadic, E.; Molina-Garcíaa, Á. Power systems with high renewable energy sources: A review of inertia and frequency control strategies over time. *Renew. Sustain. Energy Rev.* **2019**, *115*, 109369. [CrossRef]
2. Leon, A.E.; Solsona, J.A. Power Oscillation Damping Improvement by Adding Multiple Wind Farms to Wide-Area Coordinating Controls. *IEEE Trans. Power Syst.* **2014**, *29*, 1356–1364. [CrossRef]
3. Baltensperger, D.; Dobrowolski, J.; Obushevs, A.; Sevilla, F.R.S.; Korba, P. Scaling Version of Kundur's Two-Areas System for Electromechanical Oscillations Representation. In Proceedings of the 2020 International Symposium on Power Electronics, Electrical Drives, Automation and Motion, SPEEDAM, Sorrento, Italy, 24–26 June 2020.
4. Tao, F.; Qi, Q.; Nee, A. (Eds.) *Digital Twin Driven Service*; Elsevier: Amsterdam, The Netherlands, 2022.
5. Stark, R.; Kind, S.; Neumeyer, S. Innovations in digital modelling for next generation manufacturing system design. *CIRP Ann.* **2017**, *66*, 169–172. [CrossRef]
6. Pan, H.; Dou, Z.; Cai, Y.; Li, W.; Lei, X.; Han, D. Digital Twin and Its Application in Power System. In Proceedings of the 5th International Conference on Power and Renewable Energy (ICPRE), Shanghai, China, 12–14 September 2020.
7. Andryushkevich, S.K.; Kovalyov, S.P.; Nefedov, E. Composition and Application of Power System Digital Twins Based on Ontological Modeling. In Proceedings of the IEEE 17th International Conference on Industrial Informatics (INDIN), Helsinki-Espoo, Finland, 22–25 July 2019.
8. Huang, J.; Zhao, L.; Wei, F.; Cao, B. The Application of Digital Twin on Power Industry. *IOP Conf. Ser. Earth Environ. Sci.* **2020**, *647*, 012015. [CrossRef]
9. Zhou, M.; Yan, J.; Feng, D. Digital Twin Framework and Its Application to Power Grid Online Analysis. *CSEE J. Power Energy Syst.* **2019**, *5*, 391–398.
10. Brosinsky, C.; Westermann, D.; Krebs, R. Recent and prospective developments in power system control centers: Adapting the digital twin technology for application in power system control centers. In Proceedings of the IEEE International Energy Conference (ENERGYCON), Limassol, Cyprus, 3–7 June 2018.
11. Kummerow, A.; Nicolai, S.; Brosinsky, C.; Westermann, D.; Naumann, A.; Richter, M. Digital-Twin based Services for advanced Monitoring and Control of future power systems. In Proceedings of the IEEE Power and Energy Society General Meeting (PESGM), Montreal, QC, Canada, 2–6 August 2020.
12. Zolin, D.S.; Ryzhkova, E.N. Digital Twins for Electric Grids. In Proceedings of the International Russian Automation Conference (RusAutoCon), Sochi, Russia, 6–12 September 2020.
13. Montoya, J.; Brandl, R.; Vishwanath, K.; Johnson, J.; Darbali-Zamora, R.; Summers, A.; Hashimoto, J.; Kikusato, H.; Ustun, T.S.; Ninad, N.; et al. Advanced Laboratory Testing Methods Using Real-Time Simulation and Hardware-in-the-Loop Techniques: A Survey of Smart Grid International Research Facility Network Activities. *Energies* **2020**, *13*, 3267. [CrossRef]
14. Klein, M.; Roger, G.J.; Kundur, P. A Fundamental Study of Inter-Area Oscillations in Power Systems. *IEEE Trans. Power Syst.* **1991**, *6*, 914–921. [CrossRef]
15. Sattinger, W.; Ramirez, M.; Hillberg, E.; Segundo, R.; Obushevs, A.; Chacko, A.; Clauss, D.; Korba, P. Impact of aggregated assets in the power system. In Proceedings of the CIGRE Session, Paris, France, 28 September 2022.
16. Lenze. MCA Asynchronous Servo Motors. Available online https://www.lenze.com/en-ch/products/motors/servo-motors/mca-asynchronous-servo-motors/ (accessed on 17 May 2022).
17. Machowski, J.; Bialek, J.; Bumby, J. *Power System Dynamics: Stability and Control*, 2nd ed.; John Wiley & Sons, Ltd.: Hoboken, NJ, USA, 2008.
18. *IEEE Standard 115*; IEEE Guide for Test Procedures for Synchronous Machines Including Acceptance and Performance Testing and Parameter Determination for Dynamic Analysis. IEEE: Piscataway, NJ, USA, 2019.
19. Spitzer, P.; Zierhofer, C.; Hochmair, E. Algorithm for multi-curve-fitting with shared parameters and a possible application in evoked compound action potential measurements. *BioMed. Eng. OnLine* **2006**, *5*, 13. [CrossRef] [PubMed]
20. ABB. Wide Range of Applications Using Synchronous Machines up to 70 MVA. Available online: https://new.abb.com/power-electronics/excitation-and-synchronization/Unitrol-excitation-systems/unitrol-1000-series/unitrol-1010/unitrol-1000-applications (accessed on 17 May 2022).
21. NEPLAN. EXCITER MODELS: Standard Dynamic Excitation Systems in NEPLAN Power System Analysis Tool. Available online: https://www.neplan.ch/wp-content/uploads/2015/08/Nep_EXCITERS1.pdf (accessed on 20 April 2022).
22. Instruments, N. Open PMU LabVIEW Project. Available online: https://www.ni.com/en-us/support/documentation/supplemental/16/open-pmu-labview-project-.html# (accessed on 17 May 2022).
23. Python C37.118 Data Parser. Available online: https://github.com/ITI/PyMU (accessed on 17 May 2022).
24. Roscoe, A.J.; Dysko, A.; Marshall, B.; Lee, M.; Kirkham, H.; Rietveld, G. The Case for Redefinition of Frequency and ROCOF to Account for AC Power System Phase Steps. In Proceedings of the IEEE International Workshop on Applied Measurements for Power Systems (AMPS), Liverpool, UK, 20–22 September 2017.

25. Sevilla, F.R.S.; Dobrowolski, J.; Paternina, M.R.A.; Obushevs, A.; Korba, P. Examination of Wide Area Control Methods to Face Inter-Area Oscillations. In Proceedings of the 2021 World Automation Congress (WAC), Taipei, Taiwan, 1–5 August 2021.
26. Almas, M.S.; Vanfretti, L. Impact of Time-Synchronization Signal Loss on PMU-based WAMPAC Applications. In Proceedings of the IEEE Power and Energy Society General Meeting (PESGM), Boston, MA, USA, 17–21 July 2016.